Figure S1. UK021 patient lung tissues are more fibrotic with more abundance of resident macrophages than UK049 patient lung tissues. Hematoxylin and eosin (H&E) staining (400x magnification) of the freshly preserved lung tissues indicated that both NC and CA lung tissues of UK021 patient (**A**) had a higher abundance of resident macrophages that those of UK049 patient (**B**). The same trend was evident for the Gomori staining of the two sets of lung tissues for collagen (blue, 200x magnification), i.e. UK021 lung is more fibrotic than UK049 lung. This is consistent with the diagnosis of UK021 patient with COPD but not for UK049 patient.

Figure S2. β-Glucan enhances UK021 but suppresses UK049 CA lung tissue slices in releasing $^{13}C_3$-lactate into the medium. The preparation, treatment and processing of lung tissue slices were as described in **Figures 2** and **3**. Media were sampled at 0, 9 or 11 h, and 24 h during the WGP treatment in the presence of $^{13}C_6$-glucose, followed by deproteination and ^{1}H NMR analysis, as described in **Methods**. UK021 CA tissue slice released more but the UK049 counterpart released less $^{13}C_3$-lactate into the medium in a time-dependent manner. Since extracellular $^{13}C_3$-lactate represents the majority of the glycolytically produced lactate from the glucose tracer (cf. **Fig. 2** or **3** for pathway), the medium data indicated enhanced glycolysis in UK021 CA tissue slices but blocked glycolysis in UK049 tissue slices in response to WGP. The NC tissue slices for both patients displayed a decrease in the release of $^{13}C_3$-lactate into the medium, i.e. decreased glycolytic activity.

Figure S3. NMR analysis shows buildup of ^{13}C labeled metabolites of glycolysis, Krebs cycle, PPP and/or nucleotide synthesis, as well as glycogen in UK021 CA versus NC tissue slices. Slice preparation, treatment, processing, and extraction were as described in **Figure 2**. The polar extracts were analyzed by 1D ^{13}C-edited HSQC NMR for ^{13}C abundance of various metabolites at specific atomic positions, as described in **Methods**. Both control and WGP-treated spectra were normalized to the corresponding tissue wet weight for direct comparison. We observed increased ^{13}C abundance for ^{13}C-3-lactate/^{13}C-2-lactate/^{13}C-3-Ala (from glycolysis), ^{13}C-3 and 4-Glu/^{13}C-2,3-succinate (from Krebs cycle), ^{13}C-G1-glycogen (^{13}C label at C1 of the glucosyl unit of glycogen, from glycogen synthesis), ^{13}C-4-Glu-GSH+GSSG (^{13}C label at C4 of the glutamyl unit of reduced and oxidized glutathiones, from glutathione synthesis), and ^{13}C-1'-AXP (^{13}C label at C1' of the ribosyl unit of adenine nucleotides, from PPP and/or nucleotide synthesis) for the CA tissue slice in response to WGP treatment. These data are consistent with the IC-FTMS data in **Figures 2** and **4**. Decreased ^{13}C abundance of the parent glucose tracer (e.g. ^{13}C-1-α and βglucose) was also evident.

Figure S4. NMR analysis reveals depletion of ^{13}C labeled metabolites of glycolysis, Krebs cycle, PPP and/or nucleotide synthesis, as well as glycogen in UK049 CA versus NC tissue slices. Slice preparation, treatment, processing, and extraction were as described in **Figure 3**. 1D ^{13}C-edited HSQC NMR analysis was performed as in **Figure S3**. Except for glucose, the ^{13}C abundance of all other metabolites in Figure S3 showed no or opposite response to WGP in UK049 CA tissue slices, which is consistent with the IC-FTMS data in **Figures 3** and **5**.

Figure S5. NMR analysis shows that metabolic reprogramming in *ex vivo* tumors of UK021 recapitulates that in NSCLC tumors *in vivo*. Slice preparation, treatment, processing, and extraction were as described in **Figure 2**. 1D ^{13}C-edited HSQC NMR analysis was performed as in **Figure S3**. Increased ^{13}C abundance of ^{13}C-3-lactate/^{13}C-2-lactate/^{13}C-3-Ala, ^{13}C-4-Glu/^{13}C-3-acetate (surrogate for acetyl CoA), and ^{13}C-1'-AXP with decreased ^{13}C abundance of ^{13}C-G1-glycogen were evident in CA versus NC tissue slices under control treatment. These *ex vivo* metabolic distinctions between CA and NC tissues recapitulate the enhanced glycolysis, Krebs cycle, PPP and/or nucleotide synthesis observed *in vivo* in NSCLC tumors (Sellers et al. 2015).

Figure S6. NMR analysis shows that metabolic reprogramming in *ex vivo* tumors of UK049 recapitulates that in NSCLC tumors *in vivo*. Slice preparation, treatment, processing, and extraction were as described in **Figure 3**. 1D ^{13}C-edited HSQC NMR analysis was performed as in **Figure S3**. Except for an increase in ^{13}C abundance of ^{13}C-G1-glycogen, the ^{13}C-metabolic differences between the CA and NC tissue slices of UK049 had the same trend as those of UK021 (**Figure S5**), which again recapitulate the enhanced glycolysis, Krebs cycle, PPP and/or nucleotide synthesis observed *in vivo* in NSCLC tumors (Sellers et al. 2015).

Figure S7. UK021 lung tissues maintain a higher number of macrophages than UK049 lung tissues after β-Glucan treatment. WGP treatment, tissue preservation, and immunohistochemical analysis are as in **Figure 7**. Representative merged fluorescence images for CD68 and DAPI (600x magnification) are displayed in **A** for UK021 and **B** for UK049 lung tissues after 24 hr of control and WGP treatments. Both NC and CA lung tissue slices of UK021 were more abundant in $CD68^+$ cells than their counterparts of UK049.

Fig. S1

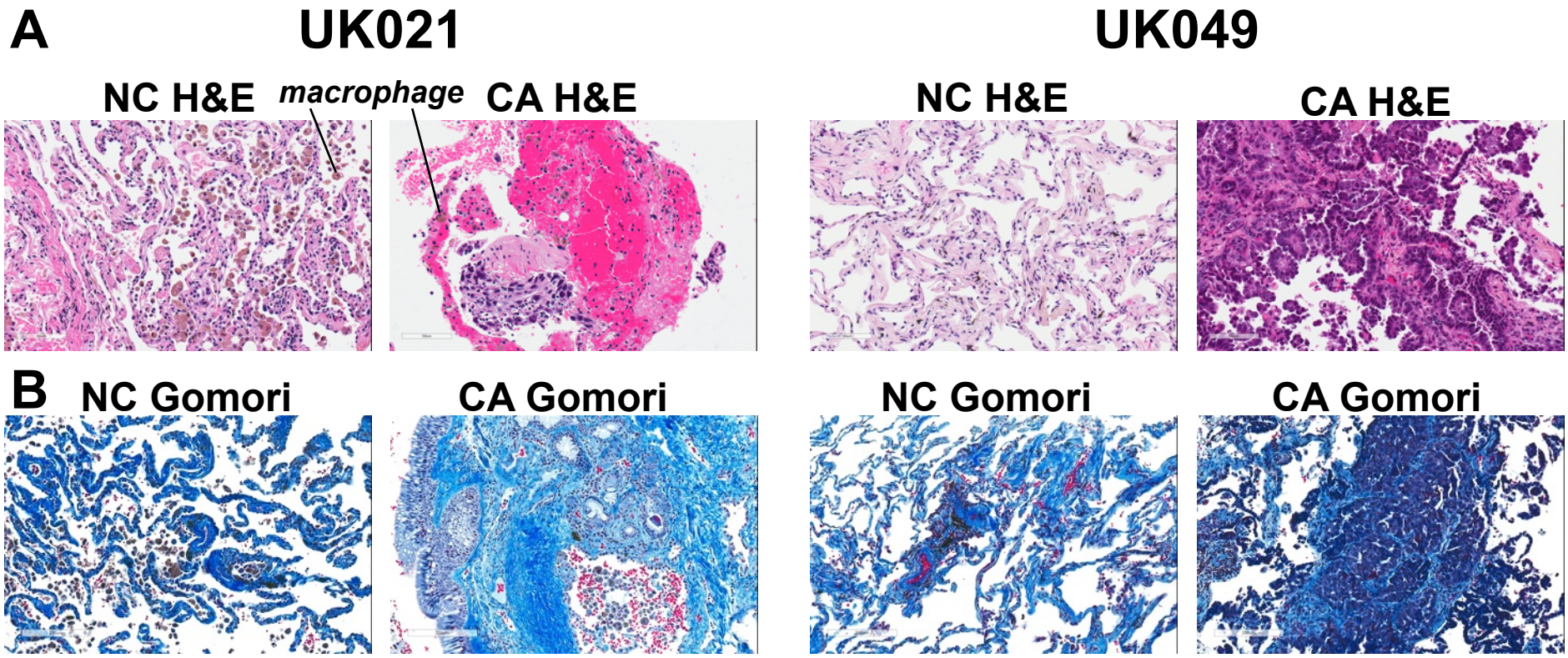
A
UK021
UK049
NC H&E
macrophage
CA H&E
NC H&E
CA H&E
B
NC Gomori
CA Gomori
NC Gomori
CA Gomori

Fig. S2

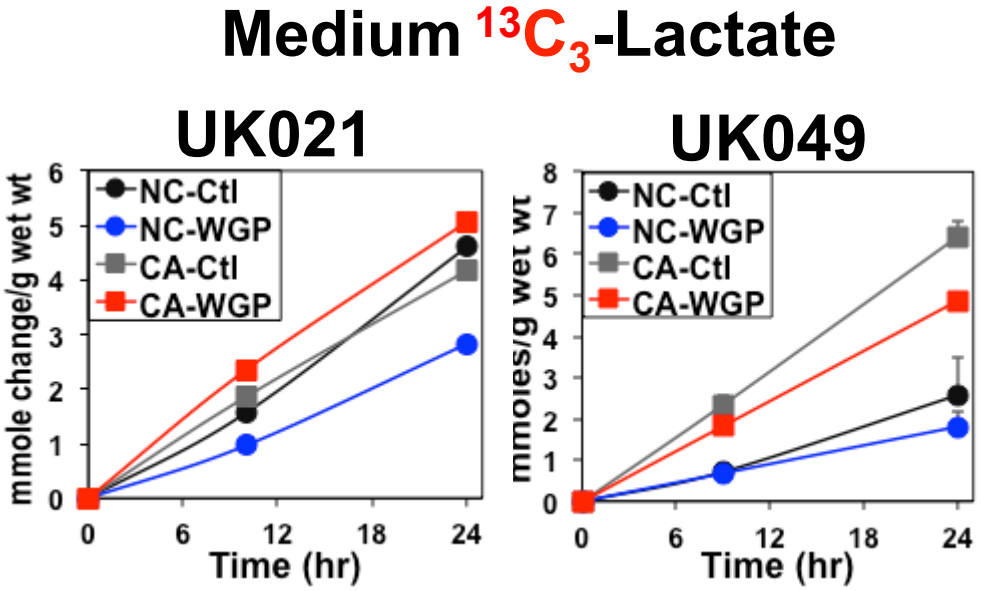
Medium $^{13}C_3$-Lactate
UK021
UK049
NC-Ctl
NC-WGP
CA-Ctl
CA-WGP
mmole change/g wet wt
mmoles/g wet wt
Time (hr)
0
6
12
18
24

Fig. S3

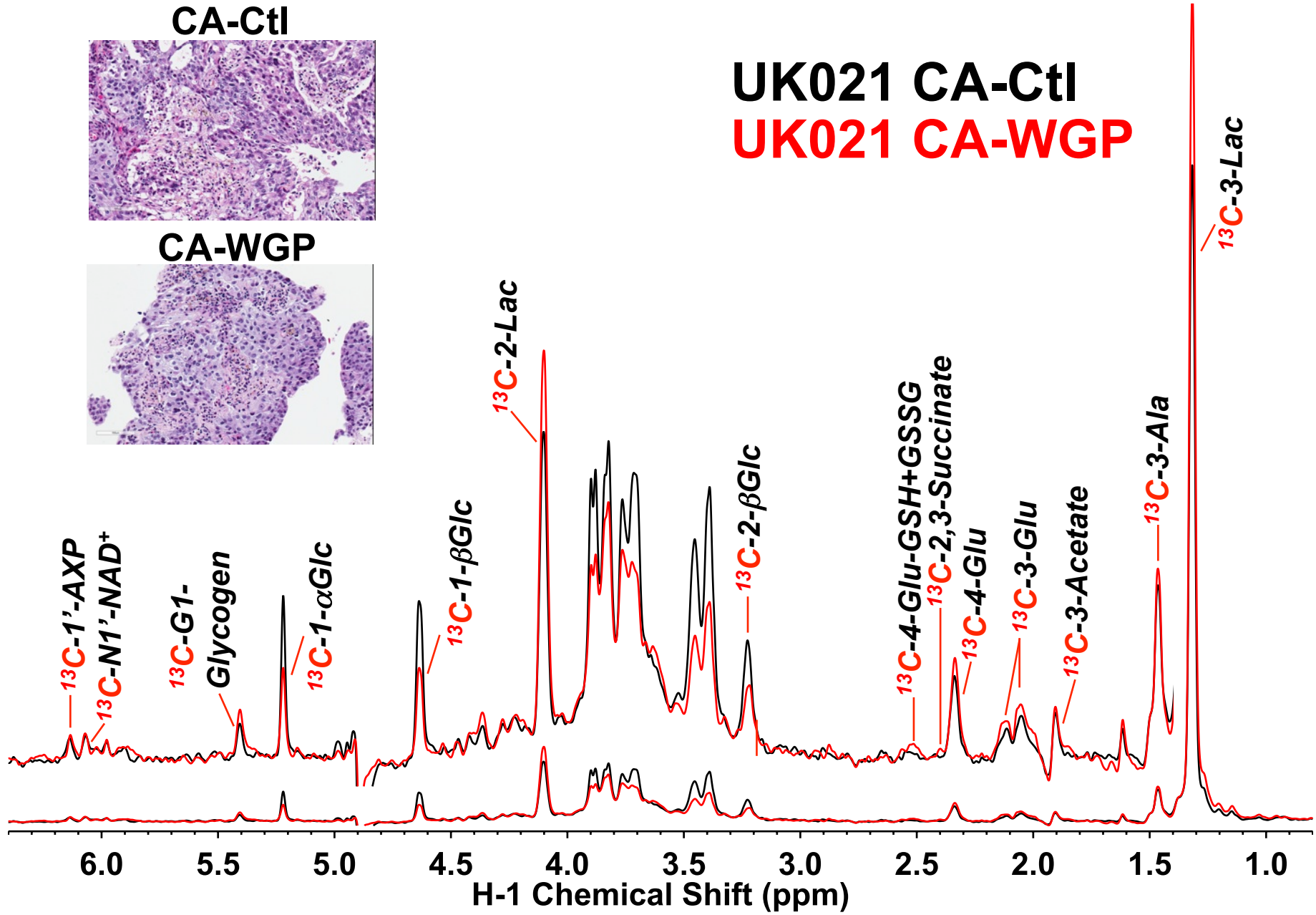
CA-Ctl
CA-WGP
UK021 CA-Ctl
UK021 CA-WGP
13C-1'-AXP
13C-N1'-NAD+
13C-G1-Glycogen
13C-1-αGlc
13C-1-βGlc
13C-2-Lac
13C-2-βGlc
13C-4-Glu-GSH+GSSG
13C-2,3-Succinate
13C-4-Glu
13C-3-Glu
13C-3-Acetate
13C-3-Ala
13C-3-Lac
6.0
5.5
5.0
4.5
4.0
3.5
3.0
2.5
2.0
1.5
1.0
H-1 Chemical Shift (ppm)

Fig. S4

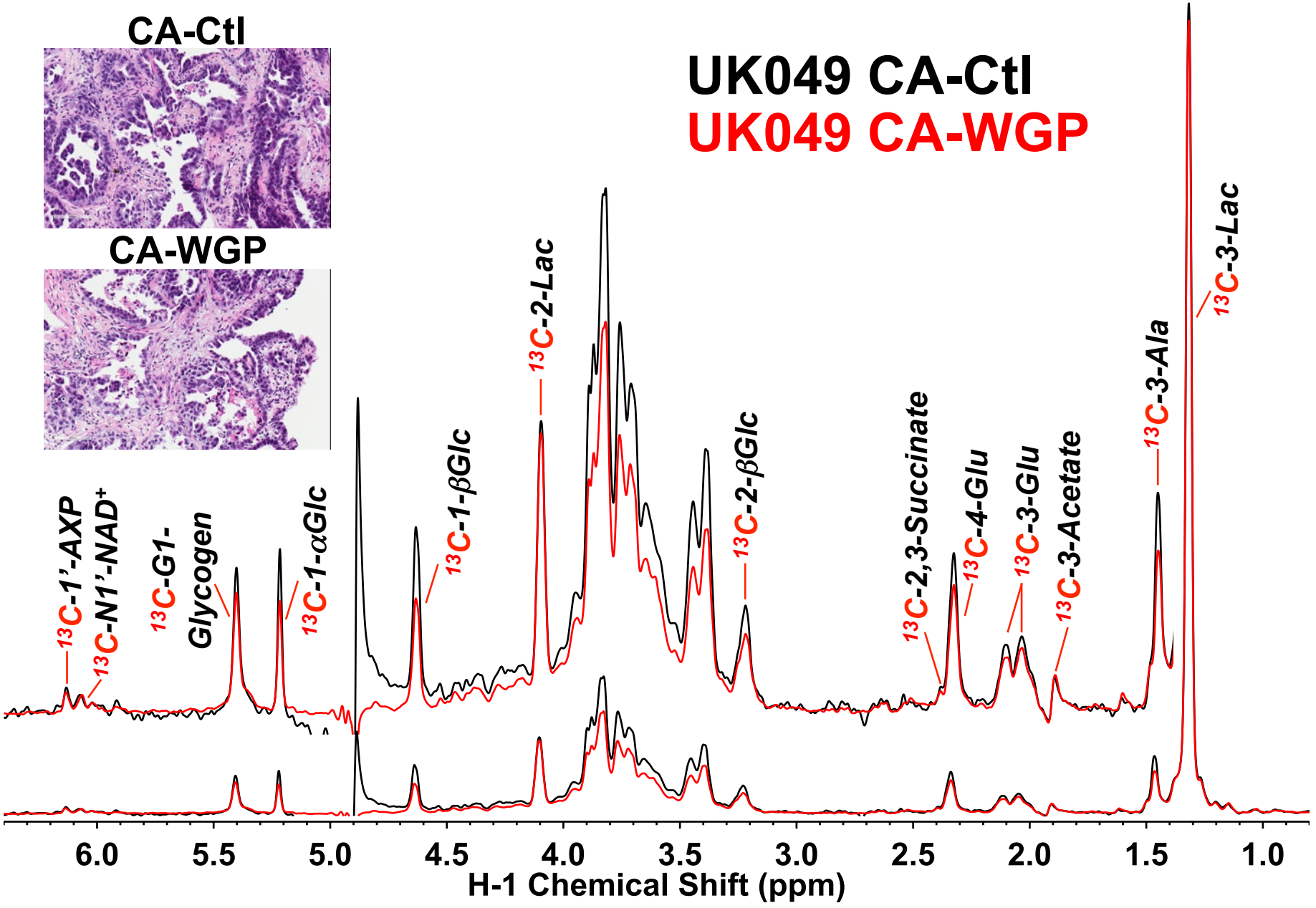
CA-Ctl
CA-WGP
UK049 CA-Ctl
UK049 CA-WGP
13C-1'-AXP
13C-N1'-NAD+
13C-G1-Glycogen
13C-1-αGlc
13C-1-βGlc
13C-2-Lac
13C-2-βGlc
13C-2,3-Succinate
13C-4-Glu
13C-3-Glu
13C-3-Acetate
13C-3-Ala
13C-3-Lac
6.0
5.5
5.0
4.5
4.0
3.5
3.0
2.5
2.0
1.5
1.0
H-1 Chemical Shift (ppm)

Fig. S5

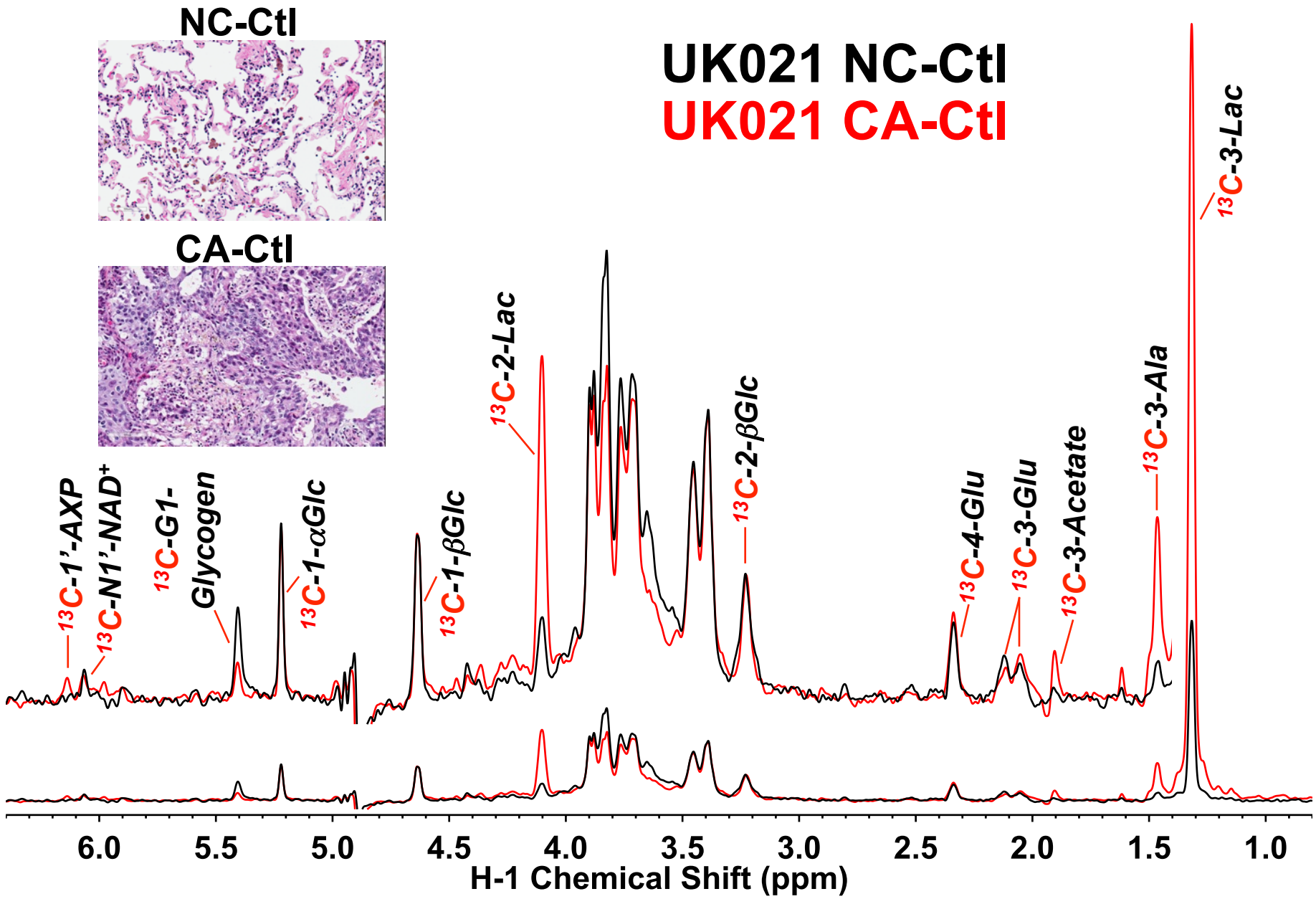
NC-Ctl
CA-Ctl
UK021 NC-Ctl
UK021 CA-Ctl
13C-1'-AXP
13C-N1'-NAD+
13C-G1-Glycogen
13C-1-αGlc
13C-1-βGlc
13C-2-Lac
13C-2-βGlc
13C-4-Glu
13C-3-Glu
13C-3-Acetate
13C-3-Ala
13C-3-Lac
6.0
5.5
5.0
4.5
4.0
3.5
3.0
2.5
2.0
1.5
1.0
H-1 Chemical Shift (ppm)

Fig. S6

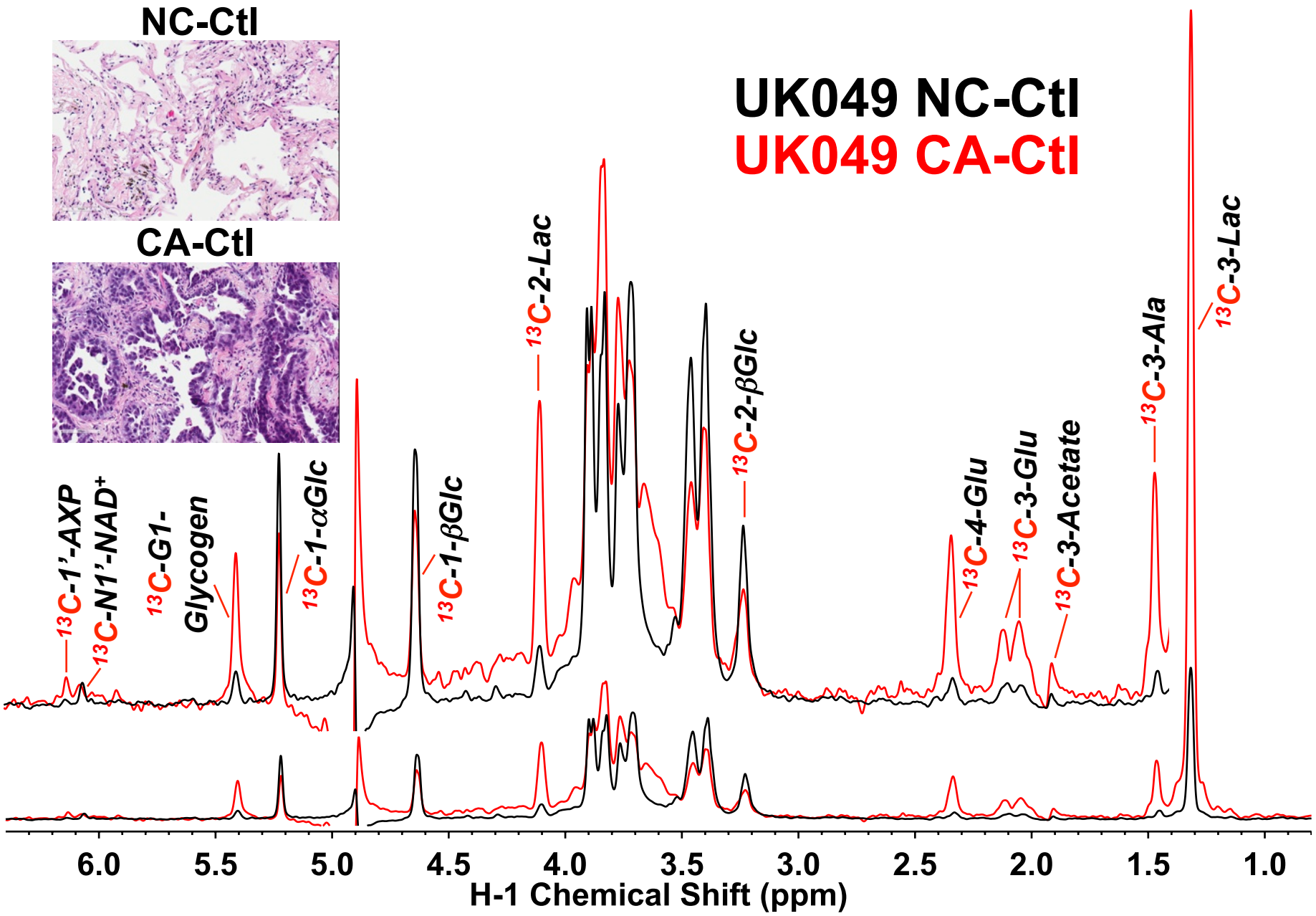
NC-Ctl
CA-Ctl
UK049 NC-Ctl
UK049 CA-Ctl
13C-1'-AXP
13C-N1'-NAD+
13C-G1-Glycogen
13C-1-αGlc
13C-1-βGlc
13C-2-Lac
13C-2-βGlc
13C-4-Glu
13C-3-Glu
13C-3-Acetate
13C-3-Ala
13C-3-Lac
6.0
5.5
5.0
4.5
4.0
3.5
3.0
2.5
2.0
1.5
1.0
H-1 Chemical Shift (ppm)

Fig. S7

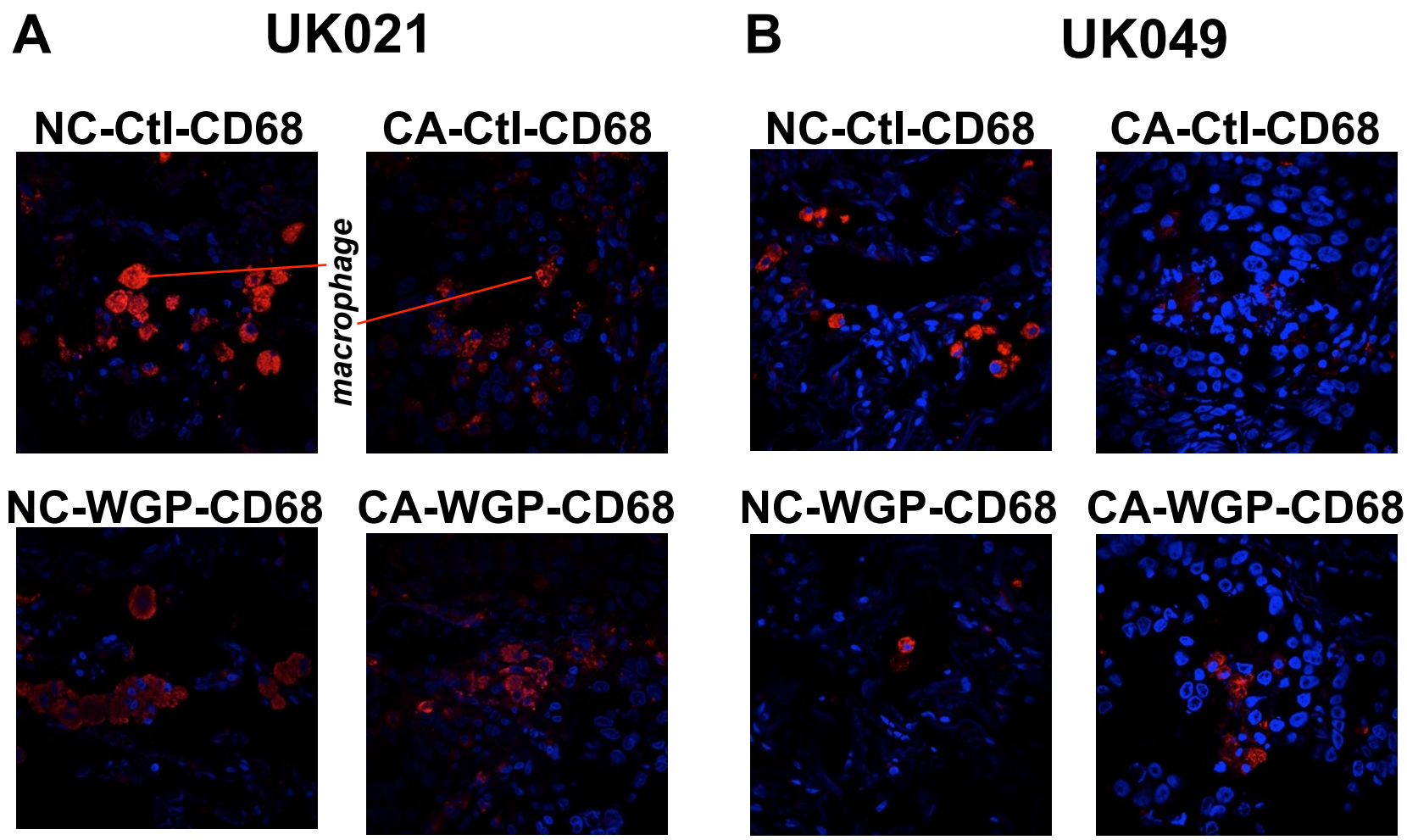
A
UK021
B
UK049
NC-Ctl-CD68
CA-Ctl-CD68
NC-Ctl-CD68
CA-Ctl-CD68
macrophage
NC-WGP-CD68
CA-WGP-CD68
NC-WGP-CD68
CA-WGP-CD68